Geophys. J. Int. (2003) **155,** 914–922

Two different methodologies for geoid determination from ground and airborne gravity data

Fadi A. Bayoud[1] and Michael G. Sideris[2]

[1] *Geodetic Engineering Laboratory, Swiss Federal Institute of Technology,* 1015 *Lausanne, Switzerland. E-mail: fadiatef.bayoud@pfl.ch*
[2] *Department of Geomatics Engineering, University of Calgary* 2500 *University Drive NW, Calgary, Canada*

Accepted 2003 July 7. Received 2003 July 7; in original form 2002 December 13

SUMMARY

In this study, two methodologies are investigated for geoid determination from ground and airborne gravity data. These two methodologies depend on the downward continuation method used. The first is the inverse Poisson integral; the second is the normal free-air gradient. Each of the two methods requires different treatment of the terrain effects and in turn different approaches to determine the geoid. The two geoid solutions, from ground data, are compared with existing GPS/levelling benchmarks and it is found that the second method gives a better fit due to the bias introduced from the inverse Poisson integral. The same process was applied to the airborne data, but with additional processing, that is the filtering of the terrain effects to preserve the consistency of the data due to the filtering of the airborne data. A study on the effect of filtering was also carried out in this paper and it concluded that filtering the terrain effects has no impact on the geoid. In addition, the airborne data, filtered to three different cut-off frequencies, were used to compute the geoid to investigate the possibility of using the denser data, of lower accuracy, to determine a high-resolution geoid. Even though the data filtered to small cut-off frequency have poorer agreement with the ground data, the geoids computed from the different filtered data is the nearly the same.

Key words: airborne gravimetry, downward continuation, geoid, GPS/Levelling, terrain correction.

1 INTRODUCTION

The methodology of geoid determination from airborne data depends, among other things, on the procedure of downward continuing the gravity data. Downward continuation can be accomplished by either inverse Poisson integral (Heiskanen & Moritz 1967), free-air gradient (Heiskanen & Moritz 1967), collocation (Moritz 1980), or analytical downward continuation (Moritz 1980). Each of these methods necessitates different methodology in computing the gravity data at the reference sphere, and in turn the geoid determination. In this study, we analyse two methodologies that take into account the downward continuation done by, first, the inverse Poisson integral that will be named the first methodology and, second, by the use of the normal free-air gradient that will be named the second methodology. As for the terrain reduction procedure, the second Helmert condensation technique is followed in spherical approximation. In the second Helmert condensation technique, all masses above the geoid are condensed to an infinitely thin layer on the geoid.

The main difference between these two methods is in the processing of the terrain effects, where the first methodology demands that the effects of the removed topographical masses and the condensed ones be evaluated at the measuring location. The second methodology requires that the effects of the removed topographical masses be evaluated at the measuring location and the condensed ones be evaluated at the reference sphere, i.e. at height zero. Two data types are used here, both located in the Canadian Rocky Mountains; the first is ground gravity anomalies, the second is airborne gravity disturbances.

In addition to testing these two methodologies, certain practical aspects of geoid determination from airborne gravity data are also studied here. Although airborne gravimetry has been used for geoid determination for a decade, some of these aspects have not yet been considered. The airborne gravity data are filtered to remove the high frequency errors coming from the dynamics of the aeroplane. Due to the low-pass filtering of the airborne data in the frequency domain, the part of the topographic gravity signal that exists beyond the filtering frequency is also filtered out. This leads to the idea that to have consistent data sets when reducing the filtered gravity signal, the contribution of the topography has to be filtered first and then be used for reduction purposes. It is the authors' opinion that although this is theoretically correct, investigation should be done to study the effect on the geoid of not filtering the terrain effects. In addition to this, the effect of Digital Terrain Model (DTM)

resolution on terrain effects computed at the flight level will be discussed. The resolutions to be studied are 15, 30, and 60 arcsec, averaged from a 3 arcsec DTM. For a comprehensive discussion, the reader can refer to Bayoud (2001).

In the following section, the respective mathematical models will be described. After that, the two methodologies will be outlined. In the last section, the conclusions are stated after comparing the geoid computed from the ground gravity anomalies with GPS/levelling benchmarks (BM) and the geoid determined from airborne gravity data with the geoid computed from the ground data (due to the lack of GPS/levelling BM in the area of the airborne data).

2 STOKES' AND HOTINE'S BOUNDARY VALUE PROBLEMS AND THEIR SOLUTIONS

Geoid determination is based on the Second Boundary Value Problem (Neumann's problem) or Third Boundary Value Problem (Robin's problem) that determines the disturbing potential on a surface, on which values functionally related to this disturbing potential exist. Stokes (1849) formulated this Neumann's problem and developed the well-known Stokes' integral for determining the disturbing potential using gravity anomalies, Δg, at the geoid. Using the Bruns formula, one can obtain geoid undulations from the computed disturbing potential. Hotine (1969), on the other hand, formulated Robin's problem by using gravity disturbances, δg, to compute the disturbing potential, and in turn geoid undulations, thus leading to Hotine's integral.

2.1 Stokes' integral

As mentioned previously, the geoid can be determined by either one of two integrals: Stokes' integral if gravity anomalies are available; or Hotine's integral if gravity disturbances are available. Since the derivation of both equations is similar and can be found in physical geodesy textbooks (e.g. Heiskanen & Moritz 1967; Hotine 1969; Dragomir *et al.* 1982), the equations will only be shown with a short discussion.

The most general form of Stokes' integral formula in spherical approximation is (Heiskanen & Moritz 1967)

$$N = \frac{k\delta M}{RG} - \frac{\delta W}{G} + \frac{R}{4\pi G}\int\int_{\sigma} \Delta g S(\psi)\, d\sigma \tag{1}$$

where k is the gravitational constant, δM is the difference in mass between the real earth and the normal earth, δW is the difference between the gravity potential of the real earth on the geoid and the normal potential of the model earth on the surface of this model, $R = 6371$ km is the radius of the reference sphere that approximates the geoid, $G = 9.80$ m s^{-2} is the mean value of gravity, Δg are gravity anomalies downward continued to the reference sphere as stated above, $d\sigma$ is the integration unit, and $S(\psi)$ is Stokes' function expressed as

$$S(\psi) = 1 + \frac{1}{\sin(\psi/2)} - 6\sin\frac{\psi}{2} - 5\cos\psi - 3\cos\psi\log\left(\sin\frac{\psi}{2} + \sin^2\frac{\psi}{2}\right) \tag{2}$$

where ψ is the spherical distance. Assuming that the mass of the real earth is equal to the mass of the normal earth and that the potentials generated from the two masses are equal, the first two terms of eq. (1) become zero.

The practical evaluation of eq. (1) can be implemented either as planar or spherical, depending on the approximation used. It can be executed in 1-D Fast Fourier Transform (FFT) or 2-D FFT (e.g. Hagmaans *et al.* 1993; Sideris & She 1992). The 1-D FFT using rigorous kernels has been applied in this paper.

Since the contribution of a Geopotential Model (GM) is subtracted from Δg, this contribution is added back in terms of geoid undulation after computing the residual geoid from eq. (1); the same is true for the topographical effects. Thus, the final geoidal height is obtained as follows:

$$N(\varphi, \lambda) = N^S(\varphi, \lambda) + N^{\mathrm{GM}}(\varphi, \lambda) + N^{\mathrm{GIE}}(\varphi, \lambda) \tag{3}$$

where the super-subscripts 'S', and 'GM' stand for the geoid components computed from Stokes' integral and the GM, respectively. N^{GIE}, on the other hand, is the topographic indirect effect and it is computed in Section 4.

2.2 Hotine's integral

Instead of using gravity anomalies, here the gravity disturbances are used. All the derivations, implementations, and modifications are similar to Stokes' integral (Hotine 1969; Novak *et al.* 2001).

Hotine's integral is written as follows:

$$N(\varphi, \lambda) = \frac{R}{4\pi G}\int\int_{\sigma} \delta g(\varphi, \lambda) H(\psi)\, d\sigma \tag{4}$$

where $H(\psi)$ is Hotine function or kernel and is described as

$$H(\psi) = \frac{1}{\sin(\psi/2)} - \log\left(1 + \frac{1}{\sin(\psi/2)}\right). \tag{5}$$

The contributions of the GM and the topography are treated in the same way as in eq. (3).

3 TOPOGRAPHIC EFFECTS

The potential of the topographical masses is given, in spherical approximation, by the equation (Martinec 1998)

$$V^t(r,\varphi,\lambda) = k\int_{\lambda'}\int_{\varphi'}\int_{R}^{R+H(\varphi',\lambda')} \frac{\rho(r',\varphi',\lambda')}{L(r,\psi,r')} r'^2 dr' \cos\varphi'\, d\varphi'\, d\lambda' \tag{6}$$

where $k = 6.672 \times 10^{-11}$ m^3 kg^{-1} s^{-2} is the gravitational constant, ρ is the density of the topography, r, φ, λ are the spherical coordinates of the computation point, r', φ', λ' are the spherical coordinates of the running integration point, $L(r,\psi,r') = \sqrt{r^2 + r'^2 - 2rr'\cos\psi}$ is the distance between the computation and running points, $\cos\ \psi = \sin\varphi\,\sin\varphi' + \cos\lambda\,\cos\lambda'\,\cos(\lambda' - \lambda)$ is the angular distance between the computation and running points, and $R = 6371$ km is the mean radius of the earth.

The above eq. (6) is handled by splitting the topography into the Bouguer shell and the irregular topography. For a thorough analysis of the above equation, the reader can refer to Martinec (1998). The final equation used for the terrain correction (TC) to gravity in the second Helmert condensation method takes the form, considering constant terrain density:

$$\mathrm{TC}(r,\varphi,\lambda) = k\rho\int\int\left[\frac{\partial\tilde{L}^{-1}(r,\psi,r')}{\partial r}\bigg|_{r'=R}^{r'=R+H(\varphi',\lambda')} - \frac{\partial\tilde{L}^{-1}(r,\psi,r')}{\partial r}\bigg|_{r'=R}^{r'=R+H(\varphi,\lambda)}\right]\cos\varphi'\, d\varphi'\, d\lambda' \tag{7}$$

The condensed TC (CTC), on the other hand, is

$$\mathrm{CTC}(r,\varphi,\lambda) = kR^2\int\int[\sigma(\varphi',\lambda') - \sigma(\varphi,\lambda)]\frac{\partial\tilde{L}^{-1}(r,\psi,R)}{\partial r}\bigg|_{r=R+H(\varphi,\lambda)}\cos\varphi'\, d\varphi'\, d\lambda' \tag{8}$$

where $\sigma\ (\varphi,\lambda)$ is the surface density of the condensation masses

$$\sigma = \rho H\left(1 + \frac{H}{R} + \frac{H^2}{3R^2}\right)$$

in the first methodology, considering that the potential of the Bouguer shell is equal to the potential of the condensed Bouguer shell, both evaluated at the measuring location (Martinec 1998).

$\sigma(\varphi,\lambda)$ is given by

$$\sigma = \rho H\left(1 + \frac{H^2}{3R(H+R)}\right)$$

in the second methodology, derived in the same way as the above equation was derived in Martinec (1998), but considering that the potential of the Bouguer shell evaluated at the measuring location is equal to the potential of the condensed Bouguer shell evaluated at the geoid.

In the computation of TC

$$\frac{\partial\tilde{L}^{-1}(r,\psi,r')}{\partial r} = [(r'^2 + 3r^2)\cos\psi + (1 - 6\cos^2\psi)rr']\tilde{L}^{-1}(r,\psi,r') + r(3\cos^2\psi)\cdot\ln|r' - r\cos\psi + \tilde{L}(r,\psi,r')|$$

is the radial derivative of the kernel

$$\tilde{L}^{-1}(r,\psi,r') = \frac{1}{2}(r' + 3r\cos\psi)\tilde{L}(r,\psi,r') + \frac{r^2}{2}(3\cos^2\psi - 1)\cdot\ln|r' - r\cos\psi + \tilde{L}(r,\psi,r')| + C \tag{8'}$$

where C is a constant.

In the computation of CTC

$$\frac{\partial\tilde{L}^{-1}(r,\psi,r')}{\partial r} = -\frac{r - r'\cos\psi}{(r^2 + r'^2 - 2rr'\cos\psi)^{3/2}}$$

is the radial derivative of the Newton kernel $1/\tilde{L}(r,\psi,r')$.

The Direct Topographic Effect (DTE) is the difference between the TC (eq. 7) and CTC (eq. 8).

Finally, the topographic indirect effect of both the actual and condensed topography is expressed as follows (Martinec 1998):

$$N^{\mathrm{GIE}}(\varphi,\lambda) = \frac{k}{\gamma(\varphi,\lambda)}\left[-2\pi\rho(\varphi,\lambda)H^2(\varphi,\lambda)\left(1 + \frac{2}{3}\frac{H(\varphi,\lambda)}{R}\right)\right.$$
$$\left. + \rho\int\int\left(\partial\tilde{L}^{-1}(R,\psi,r')\Big|_{r'=R}^{r'=R+H(\varphi',\lambda')} - \partial\tilde{L}^{-1}(R,\psi,r')\Big|_{r'=R}^{r'=R+H(\varphi,\lambda)} - R^2\frac{\sigma(\varphi',\lambda') - \sigma(\varphi,\lambda)}{L(R,\psi,R)}\right)\cos\varphi'\, d\varphi'\, d\lambda'\right] \tag{9}$$

with $\gamma\ (\varphi,\lambda)$ being the normal gravity computed from Somigliana's formula.

4 DOWNWARD CONTINUATION

4.1 Inverse poisson integral

Poisson's integral is usually used to compute gravity field functionals at a height above the earth from their values at the reference sphere.

The problem in geoid determination is the opposite. Gravity anomalies or disturbances are located at some altitude and need to be known at the reference sphere. These can be evaluated by the inverse Poisson integral.

The Poisson integral, to upward continue the gravity disturbances, is written as

$$r\delta g(r, \varphi, \lambda) = \frac{R}{4\pi} \int \int_{\sigma} \delta g(R, \varphi, \lambda) K(r, \psi, R)\, d\sigma \tag{10}$$

where $\delta g\ (r, \varphi, \lambda)$ are the upward continued gravity disturbances, $\delta g(R, \varphi, \lambda)$ are the gravity disturbances at a sphere of radius R, and

$$K(r, \psi, R) = \sum_{n=1}^{\infty} (2n+1) \left(\frac{R}{r}\right)^{n+1} P_n(\cos\psi) = R \left[\frac{r^2 - R^2}{(R^2 + r^2 - 2rR\cos\psi)^{3/2}} - \frac{1}{r} - \frac{3R}{r^2} \cos\psi \right]$$

with ψ being the spherical distance and $P_n(\cos\psi)$ Legendre function of degree n.

The solution of the inverse problem is unstable. Sun & Vanicek (1998) showed that the downward continuation of gravity disturbances (or anomalies) is well-posed when using a $5' \times 5'$ grid and an iterative scheme. This procedure is used in this study; for details see Sun & Vanicek (1998) or Martinec (1998).

4.2 Normal free-air gradient

The gravity gradient is computed from (Heiskanen & Moritz 1967)

$$\frac{\partial g}{\partial H} = -2gJ + 4\pi k\rho - 2\omega^2 \tag{11}$$

where $\frac{\partial g}{\partial H}$ is the gravity gradient sought, g is the gravity value, J is the mean curvature of a level surface and is equal to $-\frac{W_{xx}+W_{yy}}{2g}$, with W_{ii} being the partial derivative of the gravity potential along the $i-$ axis, ρ is the density of the at the location where $\frac{\partial g}{\partial H}$ is evaluated, and ω is the rotation rate of the earth.

This equation cannot be easily computed and, instead, the normal gravity gradient is used as an approximation.

The normal gravity γ at altitude h can be expanded into a series of terms of h (Heiskanen & Moritz 1967)

$$\gamma_h = \gamma + \frac{\partial \gamma}{\partial h} h + \frac{1}{2} \frac{\partial^2 \gamma}{\partial h^2} h^2 + \cdots \tag{12}$$

In this series only terms up to second order are significant. The first term of the order is approximately equal to 0.3086 mGal m^{-1}. The second can reach approximately 1.4 mGal for heights of 4325 m and is evaluated as

$$\frac{\partial^2 \gamma}{\partial h^2} = \frac{6\gamma}{a^2} \tag{13}$$

where a is the semi-major axis of the ellipsoid and γ is the normal gravity.

5 METHODOLOGIES USED FOR GEOID DETERMINATION FROM GRAVITY DATA

Depending on the method used for downward continuing the gravity disturbances (or anomalies) to the reference sphere, two methodologies are pursued to determine the geoid:

5.0.1 First methodology (Figs 1 and 3)

When the inverse Poisson integral is used, the procedure of geoid computation on the reference sphere is as follows:

(1) Compute the normal gravity at the same locations as the measured gravity values when δg is sought (or at the Telluroid; the surface whose normal potential at point q is equal to the actual potential at point p, corresponding points p and q being situated on the same ellipsoidal normal–when Δg is sought) and form δg (or Δg) values.

(2) Compute the DTE, as discussed in Section 4, at the computation point (filter them in case of airborne data), and add them to the values of step 1.

(3) Subtract the Geopotential Model contribution from the values of step 2.

(4) Downward continue the values of step 3 to the reference sphere using the inverse Poisson integral (eq. 10).

(5) Determine the co-geoid by Stokes'/Hotine's formulation (eq. 1 or 4).

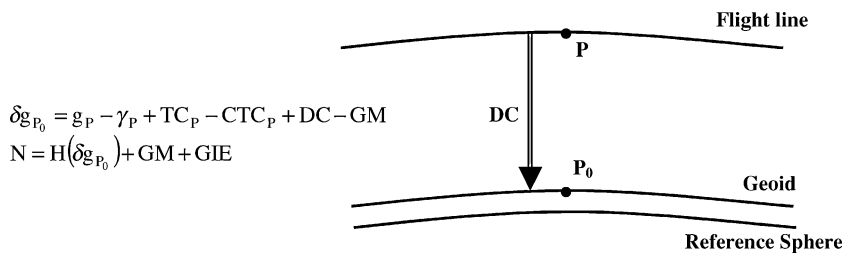

Figure 1. First methodology when computing gravity disturbances ('H' is Hotine integral).

$$\delta g_{P_0} = g_P - \frac{\partial g}{\partial H} H - \frac{1}{2}\frac{\partial^2 g}{\partial H^2} H^2 - \gamma_{P_0} + TC_P - CTC_{P_0} + DC - GM$$

$$\frac{\partial g}{\partial H} \approx \frac{\partial \gamma}{\partial h} \qquad \frac{\partial^2 g}{\partial H^2} \approx \frac{\partial^2 \gamma}{\partial h^2}$$

$$N = H(\delta g_{P_0}) + GM + GIE$$

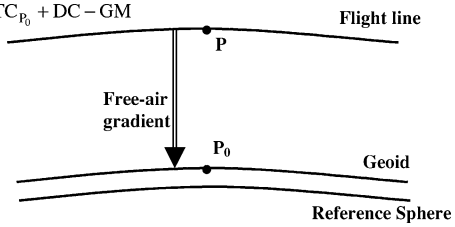

Figure 2. Second methodology when computing gravity disturbances ('H' is Hotine integral).

$$\Delta g_{p_o} = g_p - \gamma_q + TC_p - CTC_p + DC - GM$$

$$N = S(\Delta g_{p_o}) + GM + GIE$$

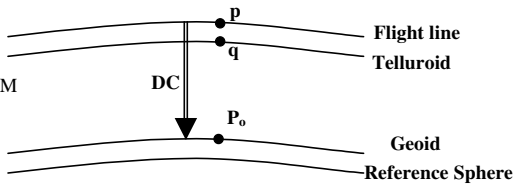

Figure 3. First methodology when computing gravity anomalies ('S' is Stokes integral).

$$\Delta g_{P_o} = g_p - \frac{\partial g}{\partial H} H - \frac{1}{2}\frac{\partial^2 g}{\partial H^2} H^2 - \gamma_{q_o} + TC_p - CTC_{p_o} - GM$$

$$\frac{\partial g}{\partial H} \approx \frac{\partial \gamma}{\partial H} \qquad \frac{\partial^2 g}{\partial H^2} \approx \frac{\partial^2 \gamma}{\partial H^2}$$

$$N = S(\Delta g_{P_o}) + GM + GIE$$

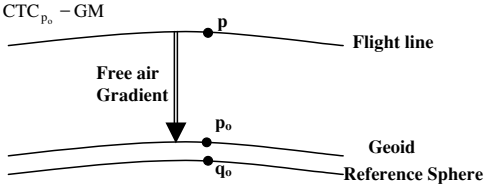

Figure 4. Second methodology when computing gravity anomalies ('S' is Stokes' integral).

(6) Compute the geoid by adding the Geoid Indirect Effect (GIE) and the GM contribution (eq. 3). The interested reader can refer to Vanicek & Martinec (1994), Martinec & Vanicek (1994a,b) for thorough analysis of this methodology.

5.0.2 Second methodology (Figs 2 and 4)

When the normal free-air gradient is used, the geoid computation on the reference sphere takes the following scheme:

(1) Compute the normal gravity at the geoid when δg is sought (or at the reference sphere when Δg is sought) and subtract it from the measured gravity values,

(2) Compute the TC (eq. 7) at the computation point (filter them in case of airborne data), and add them to the values from step 1.

(3) Compute the CTC (eq. 8) at the reference sphere (filter them in case of airborne data), and subtract them from the values from step 2.

(4) Subtract the Geopotential Model contribution from the values of step 3.

(5) Use the normal free-air gradient (eq. 12) up to the second order to downward continue the measured gravity values to the reference sphere.

(6) Determine the co-geoid by Stokes'/Hotine's formulation (eq. 1 or 4).

(7) Compute the geoid by adding the Geoid Indirect Effect (GIE) and add the GM contribution (eq. 3). The interested reader can refer to Sideris (1990) for thorough analysis of this methodology. Although the planar approximation was used in Sideris (1990), the main methodology is the same.

These two methodologies are applied when either ground or airborne gravity data is used. The only difference is in the computation of the topographic effects, where the computation point in the case of airborne data is not at the topography, but rather at the flight height. Also, when airborne gravity data is used, the topographic effects—whether they are the DTE, TC, or CTC—have to be filtered first before used in the gravity anomaly computations.

6 NUMERICAL TEST ON GROUND GRAVIMETRY

For comparing these two methodologies, we used 2110 ground gravity values located between $49.3^\circ \leq \varphi \leq 52.4^\circ$ and $241.5^\circ \leq \lambda \leq 246.5^\circ$. The refined Bouguer anomalies were used to form a $5' \times 5'$ grid between the boundaries: $49.4333^\circ \leq \varphi \leq 52.35^\circ$ and $241.875^\circ \leq \lambda \leq 246.45833^\circ$ generating 2016 values. This grid was chosen because of the availability of airborne data (for comparison) at its nodes between

Table 1. Statistics of the differences between the two gravimetric geoids and the GM after and before the fit (m).

	Max	Min	Mean	rms
first method—BM (before fit)	0.057	−1.731	−0.925	0.961
second method—BM (before fit)	0.704	−0.715	−0.314	0.467
first method—BM (after fit)	0.464	−0.728	0.000	0.170
second method—BM (after fit)	0.173	−0.401	0.000	0.096

Table 2. Statistics of TC and DTE computed from 15, 30 and 60 arcsec DTMs at the flight level of 4325 m (mGal).

		Max	Min	Mean	Std
TC	15	131.3	−73.2	1.0	30.0
	30	132.8	−73.3	1.0	30.1
	60	133.2	−73.6	1.0	30.3
DTE	15	13.2	−25.5	−0.4	6.6
	30	13.2	−25.2	−0.4	6.5
	60	12.9	−24.5	−0.4	6.4

the boundaries: $50.4333^\circ \leq \varphi \leq 51.35^\circ$ and $243.5167^\circ \leq \lambda \leq 245.0417^\circ$. For the terrain effects reduction, a 15 arcsec DTM was used; this DTM was obtained from a 3 arcsec DTM by averaging.

For an independent comparison between the two geoid solutions from the ground gravity data, GPS/Levelling BMs were used. Thirty-six Helmert orthometric heights, computed in 1995 by the Geodetic Survey Division in Canada, were used for this task. The two gravimetric geoids were interpolated, independently, at the locations of the BMs. The statistics of the differences are listed in Table 1.

As can be seen, the first methodology gives poorer agreement with the BMs (rms = 96 cm), and this is likely to be due to the magnification of the measuring error in the data due to the inverse problem, as well as to the effect of downward continuing the rough field produced by Helmert second condensation (Heck 2001). The second methodology gives an agreement of 47 cm rms.

However, after the four parameter model fit, the agreement of both methodologies improved significantly, with rms values down to 17 cm and 9 cm for the first and second methodology, respectively. The model used was:

$$D = d_1 \cos\varphi \cos\lambda + d_2 \cos\varphi \sin\lambda + d_3 \sin\varphi + d_4,$$

where D is the difference between the two data sets, φ and λ are the spherical coordinates, and the d_i's are the parameters of the surface computed by the least-squares adjustment.

7 NUMERICAL TEST ON AIRBORNE GRAVIMETRY

The airborne gravity data used here were obtained in September 1996 and are located between the boundaries $50.4333^\circ \leq \varphi \leq 51.35^\circ$ and $243.5167^\circ \leq \lambda \leq 245.0417^\circ$. The data are described in Bruton (2000). Terrain effect computations were done along the flight lines (34 560 values) at an altitude of 4325 m; the statistics are reported in Table 2.

7.1 Effect of DTM resolution on airborne gravimetry

Table 3 lists the statistics of the differences in TC and DTE, respectively, between 15 and 30, and 15 and 60 arcsec DTM. CTCs computed at the reference sphere are too small in magnitude and thus they are not affected by either the DTM resolution change or the filtering.

As it can be seen from Table 3, the airborne terrain effects are not very sensitive to the DTM resolution. A 30 arcsec DTM can be used safely without losing information at the accuracy level expected from the measuring system ($\sigma = 0.1$ mGal, max = 2 mGal). In some cases, even the 60 arcsec can be used ($\sigma = 0.4$ mGal, max = 7 mGal). From here on, we will use only data reduced to the 15 arcsec DTM.

Table 3. Statistics of the differences in TC and DTE computed from 15, 30, and 60 arcsec DTM at the flight level (mGal).

		Max	Min	Std	rms
TC	15–30	1.3	−2.1	0.1	0.1
	15–60	6.9	−3.7	0.4	0.4
DTE	15–30	1.2	−1.9	0.0	0.1
	15–60	6.1	−3.6	0.3	0.3

Table 4. Statistics of the differences between the computed and filtered TCs (mGal).

	Max	Min	Std	rms
1/30 Hz	44.5	−37.3	7.2	7.2
1/60 Hz	59.2	−50.0	12.7	12.7
1/90 Hz	92.6	−66.6	17.2	17.2

Table 5. Statistics of the differences between the computed and filtered DTEs (mGal).

	Max	Min	Std	rms
1/30 Hz	1.0	−0.7	0.1	0.1
1/60 Hz	1.6	−1.5	0.2	0.2
1/90 Hz	4.4	−4.4	0.9	0.9

7.2 Effect of filtering of terrain effects on airborne gravimetry

The TC and DTE computed from the 15 arcsec DTM were filtered to 1/30, 1/60, and 1/90 Hz cut-off frequency. The statistics of these differences are reported in Tables 4 and 5.

Regarding TC, Table 4 shows that these values are of considerable magnitude with a rms value around 13 mGal in the case of 1/60 Hz filtering. These are significant differences when computing gravity but it remains to be seen whether they have a significant effect on the geoid or not.

Table 5 illustrates the small effect of filtering the DTE; the maximum value reaches the level of 4 mGal and the rms is less than 1 mGal. These differences are smaller than the accuracy expected from the measuring system.

7.3 Geoid computed from airborne data

Now, eight data sets are formed (gridded to $5' \times 5'$), four for each methodology, as follows:

(1) Data set filtered to 1/30 Hz, reduced for filtered topographic effects to the same frequency (*data*_30).
(2) Data set filtered to 1/60 Hz, reduced for filtered topographic effects to the same frequency (*data*_60).
(3) Data set filtered to 1/90 Hz, reduced for filtered topographic effects to the same frequency (*data*_90).
(4) Data set filtered to 1/60 Hz, gridded, and then reduced for the topographic effects without filtering (*data_tc*, *data_dte*).

The first three data sets are used to investigate whether we can use the 1/30 and 1/60 Hz filtered data to achieve a high-resolution geoid. The fourth data set was formed to study the outcome of terrain effect filtering on the whole procedure. It is clear that if we do not have to filter the terrain effects, the processing becomes very easy and straightforward.

For the first methodology, these data sets were first downward continued to the reference sphere and then used to compute the geoid. In the second methodology, they were used for geoid determination right after the gridding. Note that the systematic differences with ground data were modelled and removed. Details on these systematic differences are described in Bruton (2000) and Bayoud (2001).

The eight data sets listed above were the inputs to Stokes' integral. These eight geoid solutions were compared to the geoid computed in section 6 using the second methodology as it fits the GPS/Levelling BMs better. Tables 6 and 7 show the statistics of the differences of the geoids computed from the two methodologies, respectively, and the reference geoid. Figures 5 and 6 show the representative differences of the *data*_60 geoid, from each methodology, with the reference geoid.

From the results given in these tables, we can conclude that all three frequencies, regardless of the methodology used, yield similar geoids. This means that data sets filtered to 1/30 Hz provide a geoid of similar accuracy as data sets filtered to 1/60 or 1/90 Hz, although these have better agreement with the reference gravity field. In the case under study, having a flying speed of 100 m s^{-1}, a high-resolution geoid using airborne data gridded to 3 km × 3 km can be achievable with a 5 cm rms accuracy.

Table 6. Statistics of the differences between terrestrial and airborne geoid using the first methodology (m).

	Max	Min	Std	rms
data_30	0.570	−0.332	0.165	0.218
data_60	0.616	−0.330	0.163	0.224
data_90	0.642	−0.382	0.171	0.235
data_dte	0.632	−0.331	0.164	0.227

Table 7. Statistics of the differences between terrestrial and airborne geoid using the second methodology (m).

	Max	Min	Std	rms
data_30	0.186	−0.222	0.064	0.064
data_60	0.216	−0.192	0.052	0.052
data_90	0.272	−0.220	0.061	0.061
data_dte	0.212	−0.201	0.055	0.055

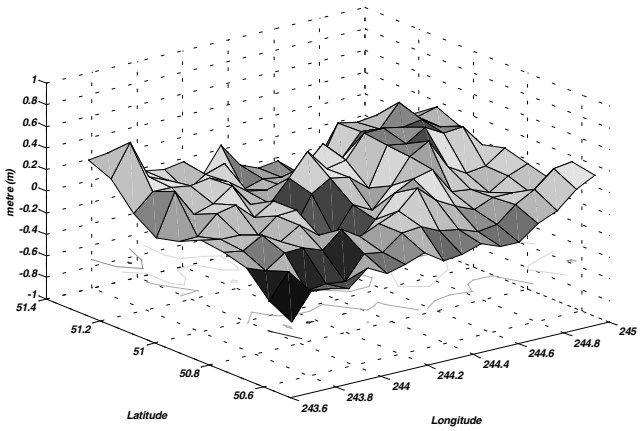

Figure 5. Differences between *geoid_60* from the first methodology and the geoid from ground data (m).

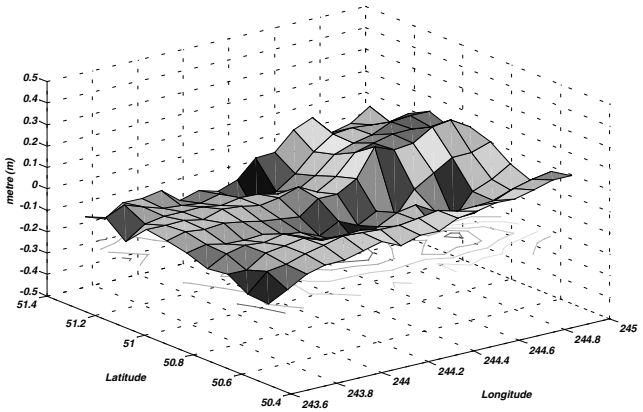

Figure 6. Differences between *geoid_60* from the second methodology and the geoid from ground data (m).

As for the fourth data set for each methodology, we conclude that filtering of the terrain effect is not needed from the practical point of view. It is enough to reduce for the terrain effect after gridding the measured gravity anomalies; a procedure that saves lots of processing time and effort.

Regarding the methodologies used, it is clear that the second methodology presents better agreement with the reference geoid, where the rms is around 5 cm; whereas that of the first methodology goes up to roughly 21 cm. This is due mainly to the nature of the inverse Poisson integral as described in Section 6.

8 CONCLUSIONS

We can state the following points:

(1) The inverse Poisson integral is less practical for computation due to the magnification of the errors in the data, and due to the rough field it generates when second Helmert condensation is used; moreover, the regularization of the inverse problem introduces a bias to the data. All these, in turn, have a consequence on the geoid. The normal free-air gradient, although an approximation, gave a geoid that is closer to the GPS/levelling BMs than the geoid determined using the inverse Poisson integral for the downward continuation.

(2) Unlike in terrestrial gravimetry, a DTM resolution of 30 arcsec in airborne gravimetry provides gravity information of the topography at the flight height with accuracy better than what the measuring system can offer. Differences in terrain effects computed from a 15 and 30 arcsec DTM are negligible. This indicates an insensitivity of the airborne gravity data to the high-frequency changes in the topography due

to the large distance of these sources from the measuring instrument. A 60 arcsec DTM can safely be used in areas with moderate topography and where high-accuracy geoid is not required. In terrestrial gravimetry the denser the DTM is, the better the geoid is determined.

(3) Although filtering of topographic effects is essential from the theoretical point of view, its effect is considerable for gravity but negligible in terms of the geoidal undulations, where this effect has an rms of less than 1 cm for filtering frequencies of 1/30, 1/60, and 1/90 Hz on a $5' \times 5'$ grid.

(4) Airborne data filtered to 1/30 Hz can provide a geoid as accurate as the 1/90 and 1/60 Hz. This would lead to a high-resolution geoid of resolution of 3 km and accuracy of 5 cm (rms). In cases when the flying speed is 50 m s^{-1}, a data set filtered to 1/30 Hz can provide an accurate geoid of resolution 1.5 km. It should be noted here that when gravity data are given on a grid denser than $5' \times 5'$, the possibility of an unstable inverse Poisson solution exists.

(5) In airborne gravimetry the geoid determined from the second methodology gave also a better fit to the geoid computed from the ground gravity data. It is believed that this is primarily due to the use of the inverse Poisson integral in the first methodology, in addition to the roughness of the field that is created when the second Helmert condensation method is used in the inverse Poisson integral.

(6) An off-the-shelf inertial navigation system integrated with the GPS can deliver a high-resolution—$5' \times 5'$—and accurate geoid, within 5 cm (rms) from a geoid computed from ground data. The same accuracy could be achieved for a resolution of 3×3 km grid when airborne gravity data filtered to 1/30 Hz is used.

ACKNOWLEDGMENTS

This work was done during the graduate studies of the first author at the University of Calgary, Dept. of Geomatics Engineering. Funding was provided by the GEOIDE Network through the second author. This is gratefully acknowledged. The downward continuation code was provided by Dr Michael Kern; this is greatly appreciated.

REFERENCES

Bayoud, F.A., 2001. Some Investigations on Local Geoid Determination from Airborne Gravity Data, *MSc thesis,* University of Calgary, Calgary, Alberta UCGE Report No. 20154.

Bruton, A., 2000. Improving the Accuracy and Resolution of SINS/DGPS Airborne Gravimetry, *PhD thesis*, University of Calgary, Calgary, Alberta. UCGE Report No. 20145,

Dragomir, V., Ghitau, M., Mihailescu, M. & Rotaru, M., 1982. *Theory of the earth's shape,* Elsevier Scientific Publishing, Amsterdam.

Hagmaans, R.E., de Min, E. & van Gelderen, M., 1993. Fast evaluation of convolution integrals on the sphere using the 1D FFT, and a comparison with existing methods for Stokes' integral, *Manuscr Geod,* **18,** 227–241.

Heck, B., 2001. On the Use and Abuse of Helmert's Second Method of Condensation, Presented in the IAG 2001 Scientific Assembly 2–7 September, Budapest, Hungary.

Heiskanen, W.A. & Moritz, H., 1967. *Physical Geodesy,* W.H. Freeman Company, San Francisco.

Hotine, M., 1969. *Mathematical Geodesy,* US. Department of Commerce, Washington, DC.

Martinec, Z., 1998. Boundary value problems for gravimetric determination of precise geoid, in *Lecture notes in Earth sciences,* Springer Verlag, Germany.

Martinec, Z. & Vanicek, P., 1994a. Direct topographical effect of Helmert's condensation for a spherical approximation of the geoid, *Manuscr. Geod.,* **19,** 257–268.

Martinec, Z. & Vanicek, P., 1994b. The indirect effect of topography in Stokes-Helmert's techniques for a spherical approximation of the geoid, *Manuscr. Geod.,* **19,** 213–219.

Moritz, H., 1980. *Advanced physical geodesy, Herbert Wichmann Verlag, Karlsruhe,* Abacus Press, Tunbridge Wells.

Novak, P., Kern, M., Schwarz, K.P. & Heck, B., 2001. The determination of the geoid from airborne gravity data, *Internal Report, Dept. of Geomatics Engineering,* University of Calgary, Calgary, Alberta UCGE Report No. 30013.

Sideris, M.G., 1990. Rigorous Gravimetric Terrain Modelling Using Molodensky's Operator, *Manuscr. Geod.,* **15,** 97–106.

Sideris, M.G. & She, B.B., 1992. A new high-resolution geoid for Canada and part of the US by the 1D-FFT method, *Bull. Geod.,* **69,** 92–108.

Stokes, G.G., 1849. On the variation of gravity at the surface of the earth, *Transactions of the Cambridge Philosophical Society*, **VIII,** 551–695.

Sun, W. & Vanicek, P., 1998. On the problems of downward continuation of the $5' \times 5'$ mean Helmert's gravity disturbances, *Journal of Geodesy,* **72,** 411–420.

Vanicek, P. & Martinec, Z., 1994. The Stokes-Helmert scheme for the evaluation of a precise geoid, *Manuscr. Geod.,* **19,** 119–128.